Available online at www.sciencedirect.com
ScienceDirect
Journal of the European Ceramic Society 31 (2011) 189–197
www.elsevier.com/locate/jeurceramsoc

Microstructural and compositional characterisation of the pyrocarbon interlayer in SiC coated low density carbon/carbon composites

Asher S. Ahmed [a], Rees D. Rawlings [a], Stephen D. Ellacott [b], Aldo R. Boccaccini [a,c,*]

[a] Department of Materials, Imperial College London, Prince Consort Rd., London SW7 2BP, UK
[b] Mersen Scotland Ltd, 11 Woodside, Eurocentral, Holytown ML1 4XL, UK
[c] Department of Materials Science and Engineering, University of Erlangen-Nuremberg, 91058 Erlangen, Germany

Received 4 November 2009; received in revised form 19 August 2010; accepted 4 September 2010

Abstract

SiC coated carbon bonded carbon fibre (CBCF) composites, a special class of carbon/carbon composites for thermal insulation, were investigated. Successful deposition of SiC requires the CBCF material to be first given a pyrocarbon coating. SiC coating on pyrocarbon coated CBCF was assessed using several analytical techniques. X-ray diffraction identified the coating as β SiC. The fibre orientation in two perpendicular planes was determined using X-ray microtomography, and it was found to be random in one plane whereas there was a preferred orientation in the other plane. A comparison was made between the uncoated and pyrocarbon coated substrates in terms of surface roughness, purity and crystallinity, using white light interferometry, neutron activation analysis/secondary ion mass spectrometry and transmission electron microscopy, respectively. The higher roughness, greater purity and increased levels of crystallinity of pyrocarbon coated CBCF are considered to be responsible for the successful deposition of a SiC coating on this material.

Keywords: B. Impurities; B. Microstructure-final; D. Carbon; E. Refractories; CBCF

1. Introduction

Carbon bonded carbon fibre (CBCF) composites are a special class of low density, highly porous carbon/carbon composites used for thermal insulation.[1] They are produced from rayon based carbon fibres which have the lowest thermal conductivity of all forms of carbon fibres and exhibit excellent refractory properties. In CBCF composites the short fibres are bonded together at the intersections of adjacent fibres with carbon char produced from carbonised phenolic powder by a high temperature heat treatment.

CBCF is a highly porous material, the typical density is in the range 0.1–0.5 g/cm^3, and its layered structure (a consequence of an early stage in the manufacturing process) means that it is anisotropic. The 2-D planar random structure of CBCF is shown in Fig. 1, and this material has been described in detail elsewhere.[2,3]

The mechanical properties of CBCF material are relatively poor but are adequate for the applications for which CBCF is used, namely thermal insulation. Properties which make these composites suitable for thermal insulation include high porosity/low density, which results in low thermal conductivity, and anisotropic thermal conductivity (higher in the direction perpendicular to the heat flow). Experimental thermal conductivity data for CBCF composites will be presented in a later study. Often, the fibres within CBCF materials are given a coating of smooth laminar pyrocarbon using a chemical vapour deposition (CVD) process. This coating provides improved mechanical properties to the CBCF,[2,3] and the material is then called CVD CBCF. CBCF composites can also be produced with a high level of purity (<0.2%), which is important in applications such as high purity single crystal growing furnace insulation, as any impurities in the insulation can contaminate the crystals being grown.

* Corresponding author. Tel.: +49 9131 8528601; fax: +49 9131 8528602.
E-mail addresses: aldo.boccaccini@ww.uni-erlangen.de, a.boccaccini@imperial.ac.uk (A.R. Boccaccini).

0955-2219/$ – see front matter © 2010 Elsevier Ltd. All rights reserved.
doi:10.1016/j.jeurceramsoc.2010.09.004

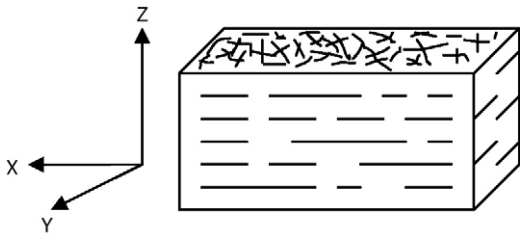

Fig. 1. 2D planar random structure of CBCF material.

The usage of CBCF based materials has been limited within the thermal insulation sector due to problems with oxidation (carbon/carbon composites oxidise readily above around 450 °C[4]) and degradation within other hostile environments such as a hydrogen atmosphere which can lead to the formation of methane. This reactivity means that CBCF materials are currently only used in applications which involve an inert atmosphere or vacuum.

In an attempt to improve the performance of CBCF materials within these reactive environments, prototype materials have been produced where CBCF and CVD CBCF substrates have been infiltrated with a protective coating of silicon carbide using chemical vapour deposition. The silicon carbide coating does not encapsulate the substrate, rather the entire porous framework is infiltrated and coated. The CVD of silicon carbide is only successful when employing CVD CBCF as the substrate. When silicon carbide deposition has been attempted with CBCF substrates (i.e. with no pyrocarbon layer), the samples have disintegrated into green powder. It should be noted that within this paper, the silicon carbide coated CVD CBCF substrate material is, for simplicity, referred to as silicon carbide coated CBCF. To date no information is available on either the microstructure or the properties of the silicon carbide coated CBCF material.

The present work is the first characterisation study of the silicon carbide coated CBCF material focusing on material microstructure and on the effect of the pyrocarbon layer on the SiC coating. A variety of techniques, including scanning and transmission electron microscopy, X-ray diffraction and X-ray microtomography, were used. Explanations have also been sought as to why silicon carbide deposition is only successful for the CVD CBCF and not for the uncoated base CBCF material. Avenues of investigation included a comparison of the relative purity levels, surface roughness and crystallinity of the two substrates (CBCF and CVD CBCF).

2. Experimental procedure

2.1. Manufacture of materials

The production of CBCF materials has been described in detail elsewhere.[1] A flow diagram of the manufacturing process is shown in Fig. 2. The CVD process used to deposit pyrocarbon onto CBCF (forming CVD CBCF) is conducted at 1000–1100 °C, and employs nitrogen as the carrier gas and methane as the precursor gas. Typically, a 0.25 μm thick pyrocarbon coating has been deposited for the materials investigated in this study. The CBCF materials were manufactured and supplied by Mersen Scotland Ltd, UK. The infiltration of SiC was carried out by means of an industrial CVD process using methyltrichlorosilane (MTS) as the precursor gas. All results for silicon carbide coated materials within this paper are for the CVD CBCF substrate, as when attempts at deposition were made using the CBCF material, the samples lost their structural integrity and were not suitable for testing. The composite is denoted as silicon carbide coated CBCF.

2.2. Characterisation of microstructure

Samples for scanning electron microscopy (SEM) were prepared by cutting cubes using a scalpel and mounted on metal stubs using carbon tape. The electrical conductivities of all samples (CBCF, CVD CBCF and silicon carbide coated CBCF) were sufficient for examination without prior coating. Typically, SEM samples would have dimensions of 5 mm × 5 mm × 5 mm. The samples were examined in a JSM5610LV SEM at acceleration voltages ranging from 5 to 30 kV.

The transmission electron microscope (TEM) used was a JEOL 2000FX TEM. TEM samples were prepared using a focused ion beam generated by a FEI FIB200-SIMS, ion microscope. The first step was to attach fragments of the silicon carbide coated CBCF to copper grids. The grids were placed within the apparatus and suitable regions within the fragments were located and then thinned using the beam.

X-ray diffraction (XRD) analysis was conducted on the silicon carbide coated CBCF material. The diffractometer used was a Philips PW2273 diffractometer, and it was operated at 40 kV and 40 mA with a copper tube to give copper K_α radiation. The samples were cut using a scalpel and were tested in block form with dimensions of 3 mm × 5 mm × 5 mm. The scans were conducted for 2θ values between 0° and 90°, at increments of 0.04°, with each increment lasting for 1 s.

The fibre orientation within the silicon carbide coated CBCF material was determined using X-ray microtomography (XMT).

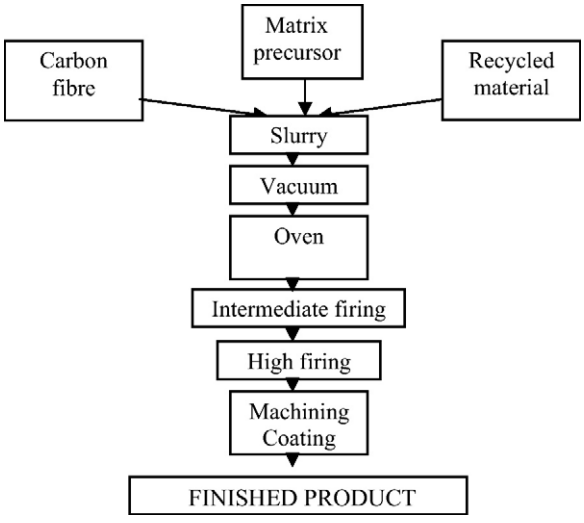

Fig. 2. Flow diagram summarising the manufacturing process for CBCF materials.

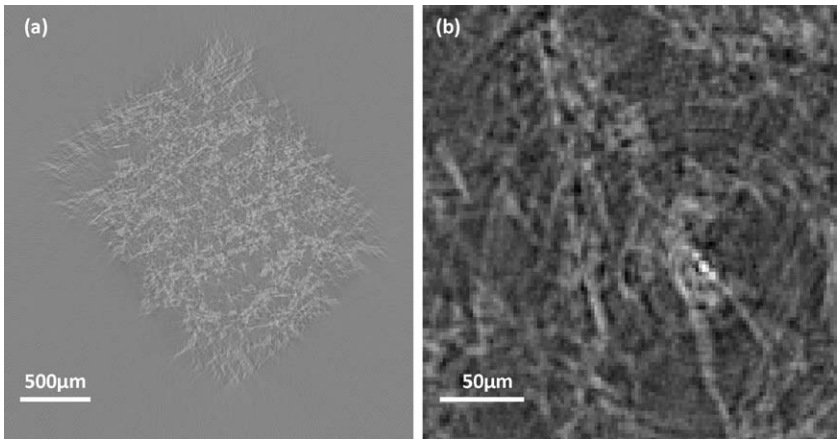

Fig. 3. XMT images of a silicon carbide coated CBCF sample (*z* orientation) used for studying fibre orientation showing (a) an entire slice within the sample and (b) a higher magnification image of fibres within the slice.

The XMT unit used was a 'v|tome|x s' type manufactured by Phoenix X-ray Systems and Services GmbH (Munich, Germany). The samples for XMT analysis were blocks with dimensions of 5 mm × 5 mm × 5 mm. The XMT data were analysed using Image J software and the fibre orientations were determined as follows: the contrasts of the images were optimised and the noise levels were minimised as far as possible. The angle tool was then used to determine the angle of individual fibres with respect to the vertical. The XMT data were divided into 512 slices. The angles for 20 fibres were measured within 50 slices at varying positions within the sample. This was done for both the *x*/*y* and *z* orientation. The CBCF materials were on the limits of resolution for the XMT apparatus. Fig. 3 shows typical XMT images where (a) shows an entire slice within the silicon carbide coated CBCF sample and (b) is a higher magnification image of a region within this slice.

In order to establish whether the surface roughness of the carbon fibres within the CBCF composite structure is different to that of the CVD carbon coated fibres, the two materials were examined using a white light interferometer (Zygo NewView 200 white-light microscope-based interferometer). Two samples were looked at for each material with roughness profiles taken for 20 fibres within each sample. These fibres were from different regions within the respective samples. Thus a total of 40 fibres were looked at for the CBCF and 40 fibres for the CVD carbon coated surface. All profiles were taken along fibre lengths, and were at least 50 μm long. The parameters used to assess the roughness of the surfaces were the average roughness (R_a), the root mean square roughness (R_{rms}) and the peak-to-valley roughness (R_{PV}).

2.3. Compositional analysis

Neutron activation analysis (NAA) involves bombarding samples with a stream of neutrons resulting in the absorption of neutrons by the nuclei of the various elements present within the sample, thus forming radioactive isotopes. The emissions from these isotopes, which are unique for the various elements as the elements emit radiation with different energies and at different durations to achieve stability, are then monitored/analysed and used to determine the elemental composition of the sample. NAA provides data for the entire sample and not just the surface facing the neutron beam, as the neutrons are able to penetrate deep into the sample. The NAA for the current study was conducted at the NAA facility at the Imperial College Reactor Centre, UK. One sample was tested for both the CBCF and the CVD CBCF materials. Samples were cut using a sterilised scalpel and handled using nitrile powderless gloves in order to minimise contamination. The samples had to fit into a capsule of 17 mm diameter and 27 mm height and were thus cut with dimensions of 10 mm × 10 mm × 25 mm. The neutrons for irradiation were generated by chained uranium-235 fission reactions, and both samples were subjected to a short (1 day) as well as a long (3 days for irradiation and then gamma-ray analysis after 10 days) NAA. The emitted gamma rays from the various elements present within the samples were detected by a GAMMA-X Germanium (HPGe) Coaxial Detector.

Secondary ion mass spectrometry was conducted using a FIB SIMS apparatus (FEI FIB200-SIMS) which employed gallium ions (Ga^+) of energy of 30 keV to bombard the samples. The sputtered ions from the sample were detected using an electric quadrupole mass spectrometer. Two samples were prepared, one for the CBCF material and the other for the CVD CBCF material. Again, great care was taken during sample preparation in order to prevent contamination, i.e. using a sterilised scalpel and nitrile powderless gloves. The sample dimensions were 50 mm × 10 mm × 10 mm.

Three different approaches were taken for SIMS analysis. The first was where regions within both samples (CBCF and CVD CBCF) were scanned for all elements with relative atomic masses (A_r) ranging from 0 to 100. This was done within five different regions for both samples. These regions were located along the length of five different fibres for the CVD CBCF sample, whereas for the CBCF, three of the regions were along fibre lengths and two were on fibre ends. Typical scanned areas were 100 μm^2 along fibre lengths and 40 μm^2 on the fibre ends. Mean values were then calculated for all impurities deemed to be present in significant quantities.

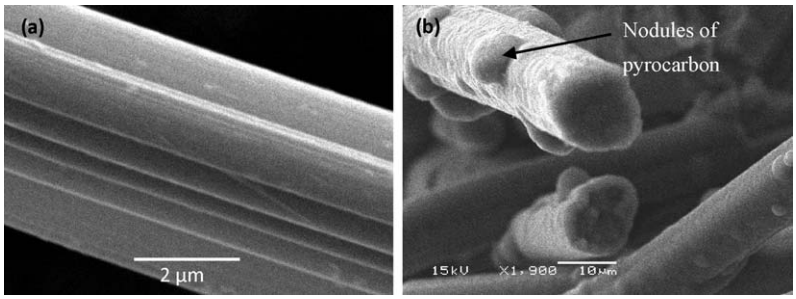

Fig. 4. SEM images showing (a) the crenulated structure of a carbon fibre produced from rayon precursor and (b) carbon fibres coated with pyrocarbon.

The second approach was depth profiling. This involved scanning for certain elements of interest and determining how the counts, and hence concentrations, changed with increasing depth. Typically, an area of 100 μm^2 was scanned to a depth of approximately 1 μm, at a rate of 0.1 μm/min. Only the coated material, CVD CBCF, was depth profiled, as the intention was to see how the impurities changed on passing from the coating to the body of the fibre. The elements studied were based on the NAA results, and also to a lesser degree on the SIMS results from the first approach, and were: aluminium, silicon, calcium, titanium, chromium and iron. Eight different fibres were scanned for aluminium, silicon and calcium, and three different fibres were scanned for titanium, chromium and iron.

The final approach was digital mapping of fibres within the CVD CBCF material (i.e. coated fibres). The pixel darkness within these mappings corresponds to the intensity of the element being investigated and each image map consisted of 256 × 220 pixels. The measurement time was 4 ms per pixel hence each mapping took approximately 4 min. Mappings were obtained for the same 'elements of interest' as for the depth profiling, namely: aluminium, silicon, calcium, titanium, chromium and iron. Four different regions were scanned, where region 1 contained two fibre ends, and regions 2, 3 and 4 contained solitary fibres.

3. Results and discussion

3.1. Structure characterisation

The carbon fibres used to produce CBCF materials are manufactured from a rayon precursor, and have a crenulated, 'celery-like' structure. Fig. 4a shows an uncoated carbon fibre within a CBCF sample which illustrates this structure. Once the CBCF material has been given the pyrocarbon coating (forming CVD CBCF), the fibres become more cylindrical (Fig. 4b). The pyrocarbon coating deposited is relatively uniform but nodules of pyrocarbon are also present (indicated by arrow in Fig. 4b).

SEM conducted on the silicon carbide coated CBCF showed that good coverage of the silicon carbide had been achieved throughout the CVD CBCF substrate (Fig. 5a), and that the silicon carbide coating was of sound quality in that it had few flaws (i.e. no large pores or cracks) within the protective system. The surface of the deposit was however coarse in nature (Fig. 5a and b). In Fig. 5b the various constituents of the silicon carbide coated CBCF composite can clearly be seen, namely the carbon fibres, pyrocarbon and silicon carbide coatings, as indicated by the arrows. The average thickness of the SiC coating on the fibres was 1 μm.

Fig. 6a is a TEM image showing the carbon fibre, pyrocarbon and silicon carbide coatings. The SiC deposit consists of two regions; the first of these is a fine polycrystalline region, approximately 0.3–0.4 μm in thickness, formed as a consequence of a high nucleation rate on the pyrocarbon substrate. Out of this fine grained layer larger columnar silicon carbide grains have grown (∼0.5 μm in size), presumably at an orientation with a high growth rate, giving an overall SiC thickness of about 1 μm, which is consistent with the SEM observations (Fig. 5a and b). The faults that can be seen perpendicular to the growth direction within the large columnar grains are typically seen for a (1 1 1) growth direction for β silicon carbide. Fig. 6b is a higher resolution TEM image showing the two interfaces within the silicon carbide coated CBCF material, i.e. the carbon fibre–pyrocarbon interface and the pyrocarbon–silicon carbide interface. Note how the latter appears to be rougher than the former.

Fig. 7 is a high resolution TEM image of the carbon fibre–pyrocarbon interface, where the carbon fibre is on the

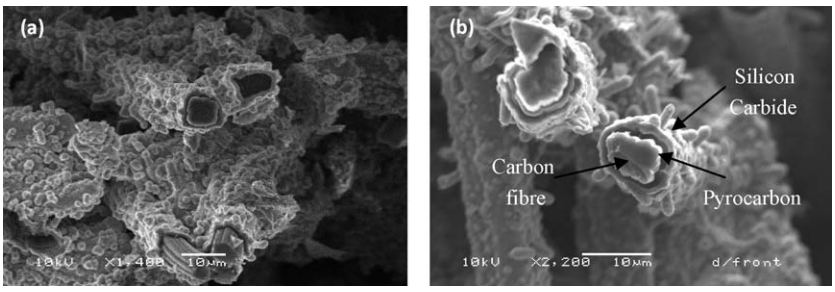

Fig. 5. SEM images showing the silicon carbide coated CBCF material.

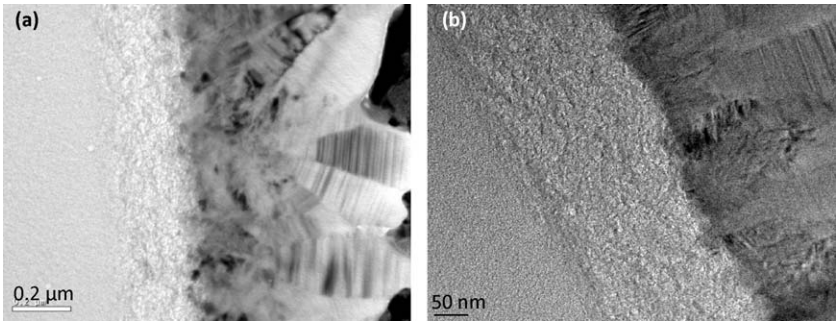

Fig. 6. TEM images of the silicon carbide coated CBCF showing (a) the carbon fibre, pyrocarbon and silicon carbide coatings and (b) a higher magnification image of the interfaces.

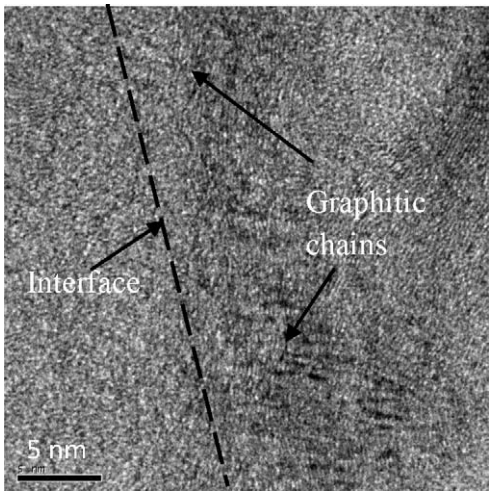

Fig. 7. HRTEM image showing carbon fibre and pyrocarbon in SiC coated CBCF composite.

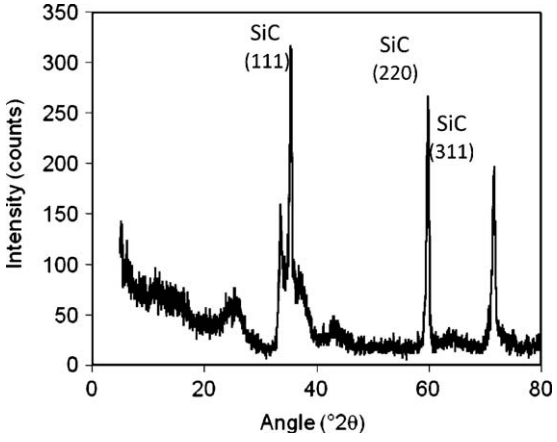

Fig. 9. X-ray diffraction trace for a silicon carbide coated CBCF specimen.

left of the image and the interface is delineated by a dashed line. The pyrocarbon can be seen as being more crystalline than the amorphous carbon fibres with a greater extent of graphitic chain formation (darker regions, indicated by arrows). Fig. 8a and b shows electron diffraction patterns yielded for the carbon fibres and pyrocarbon coating, respectively. The fact that the amorphous ring has become sharper for the pyrocarbon is indicative of the greater crystallinity and increased structuring of the pyrocarbon deposit when compared to the carbon fibres.

XRD analysis demonstrated that the silicon carbide being deposited was β-SiC with strong (1 1 1), (2 2 0) and (3 1 1) diffraction peaks (see Fig. 9). Previous workers have also reported this crystal structure for CVD silicon carbide.[5,6]

Fig. 10a and b shows the fibre orientations (represented as percentage of fibres lying at a particular angle) for the silicon carbide coated CBCF determined using XMT for the *x*/*y* and *z* orientations, respectively. The angles were determined for fibres with a minimum visible length of 20 μm, and the angle was that formed between the leading edge of the fibre and a vertical line (representing 0–180°). The study was undertaken to demonstrate the random orientation of fibres within the *x*/*y* planes, and the preferred orientation in the *z* orientation. The

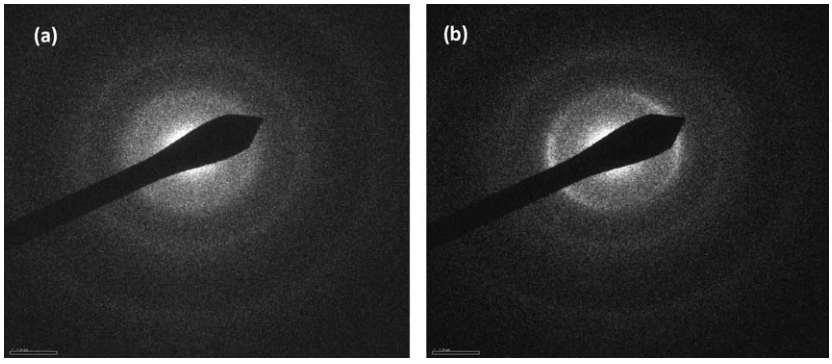

Fig. 8. Electron diffraction patterns of (a) carbon fibre and (b) pyrocarbon in SiC coated CBCF composite.

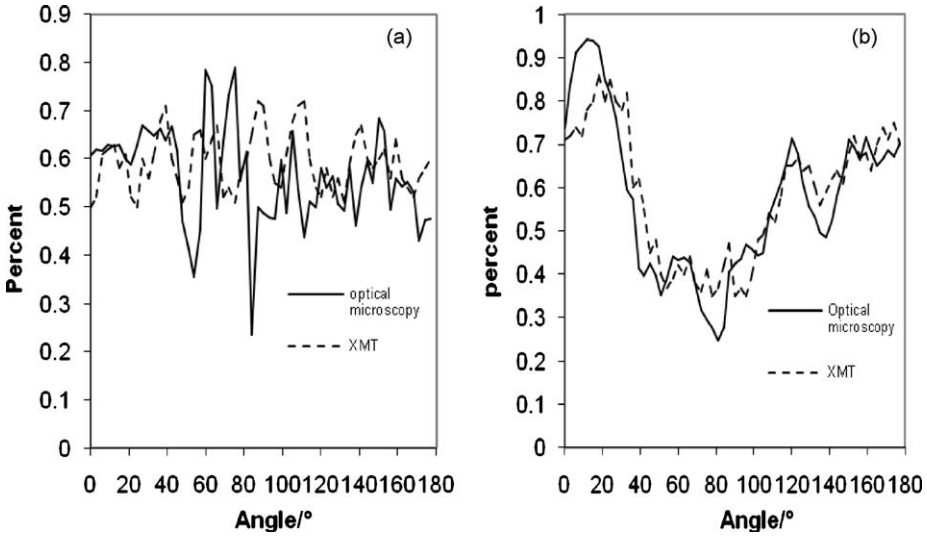

Fig. 10. Angles of the fibres within CBCF materials measured using optical microscopy and XMT for (a) the *x*/*y* orientation and (b) the *z* orientation.

figures also show fibre orientations determined in a previous study using optical microscopy.[1] These values were determined for the CBCF material with either 0 or 100% recycled material incorporated in the composite. It is known that the amount of recycled material incorporated in CBCF composites has an influence on the resulting microstructure of the material.[7] This behaviour is particularly so at higher percentages of incorporated recycled material (>85%), where the resulting materials become increasingly isotropic. As the materials studied in the current investigation contain approximately 15% recycled material, the values from Ref. [1] were modified as follows: the 0% recycled material value was subtracted from the 100% value and the difference multiplied by 0.15 (as materials being investigated in this study contain 15% recycled material). This value was then added to the 0% recycled material value. This was done for all the angles and for both the *x*/*y* and the *z* orientations to produce the optical microscopy data presented in Fig. 10. There is good agreement between the fibre directions measured using XMT and the values modified from the work reported in Ref. [1]. The graphs also show how the fibres within the *x*/*y* layers are randomly orientated, whereas the fibres in the *z* orientation tend not to lie horizontally (not at angles ranging from 40° to 100°).

The surface roughness parameters determined using the Zygo® white light interferometer for the CBCF and CVD CBCF materials are presented in Table 1. These parameters clearly show that the surface of the CVD CBCF is much rougher than that of the CBCF material.

3.2. Compositional analysis

The results of the neutron activation analysis conducted for the CBCF and CVD CBCF samples are shown in Table 2. Only elements detected with concentrations greater than 1 mg/kg have been included. The CVD CBCF material can be seen as being considerably purer than the CBCF material, which reflects the low level of impurities of the pyrocarbon being deposited. The major impurities within CBCF materials are: aluminium, silicon, sulphur, chlorine, calcium, titanium, chromium, iron and barium.

Table 3 shows the counts for various elemental impurities yielded via the general SIMS analysis for the CBCF and CVD CBCF (only elements present in significant quantities have been included). The standard deviations for these measurement are high nevertheless the data indicates that for most elements the counts are lower for the CVD CBCF in agreement with the NAA results. Differences between results generated using SIMS and NAA are due to either the fact that SIMS is analysing the surface of samples whereas NAA is studying the bulk sample, or the differing sensitivities of the techniques to the various elements.

Fig. 11 shows three of the SIMS depth profiling traces obtained for calcium. Although eight traces were obtained for calcium, six of the traces were similar to trace 1, i.e. they exhibited an increase in count on passing to the fibre. The other two traces (trace 2 and trace 3 in Fig. 11) showed similar count in fibre and coating. All calcium traces had a jump in counts at the interfacial region, reflecting a higher level of impurity at

Table 1
Roughness parameters for the CBCF and CVD CBCF materials determined using a Zygo® white light interferometer.

	R_a (μm)		R_{rms} (μm)		R_{PV} (μm)	
	CBCF	CVD CBCF	CBCF	CVD CBCF	CBCF	CVD CBCF
Mean	1.64	2.55	2.09	3.16	8.79	13.2
95% Confidence interval for mean	1.21–2.08	2.11–2.99	1.58–2.60	2.65–3.67	6.52–11.1	10.9–15.5
Standard deviation	0.94	1.73	1.15	1.99	5.58	8.53

Table 2
Impurities within the CBCF and CVD CBCF composites as determined using neutron activation analysis.

Concentration		
Impurity	CBCF (mg/kg)	CVD CBCF (mg/kg)
Na	<3.4	<2.8
Mg	<12	<1.0
Al	18 ± 1	19 ± 1
Si	<900	<500
S	<1200	<470
Cl	<19	<11
Ca	190 ± 15	120 ± 9
Ti	46 ± 2	11 ± 1
Cu	<1.6	<0.81
Ge	<2.1	<1.2
Sr	2.6 ± 0.9	1.3 ± 0.4
Nb	<21	<11
Ru	<3.6	<2.1
Sn	<2.3	<1.3
Pt	<3.9	<2.1
Hg	<12	<6.3
Th	<1.3	<1.0
K	4.3 ± 0.8	1.2 ± 0.3
Cr	51 ± 2	3.7 ± 0.2
Fe	<133	<83
Ni	7.0 ± 1.3	4.3 ± 0.8
Zn	<1.2	<0.74
Mo	1.2 ± 0.3	0.43 ± 0.16
Ba	141 ± 9	77 ± 5

the fibre surface/interfacial region. This jump at the interfacial region was only seen for calcium and a few aluminium traces. As shown in Fig. 11, there was some variability in the depth profiling traces for a given element, but in general the traces for the various elements (silicon, calcium, titanium, chromium and iron) exhibited an increase in counts with increasing depth. Aluminium was the exception as six out of eight traces showed a decrease with depth. Overall, the depth profiles confirm that the pyrocarbon is purer than the fibres.

Table 3
Impurity counts for the CBCF and CVD CBCF materials determined using secondary ion mass spectrometry.

Element	relative atomic mass (A_r)	CBCF	CVD CBCF
Na	22.99	12 ± 6	22 ± 23
Mg	24.30	13 ± 6	12 ± 5
Al	26.98	24 ± 10	29 ± 29
Si	28.09	19 ± 7	14 ± 11
P	30.97	18 ± 9	11 ± 8
S	32.07	5 ± 2	3 ± 1
Cl	35.47	6 ± 2	4 ± 1
K	39.10	26 ± 10	56 ± 58
Ca	40.09	158 ± 177	55 ± 13
Ti	47.88	5 ± 1	3 ± 1
Cr	51.94	7 ± 2	3 ± 1
Fe	55.85	14 ± 11	6 ± 4
Ni	58.69	4 ± 2	3 ± 2
Co	58.93	6 ± 3	4 ± 2
Sr	87.62	10 ± 7	7 ± 5
Mo	95.94	3 ± 1	3 ± 1

The SIMS digital mapping for the various elements (aluminium, silicon, calcium, titanium, chromium and iron) showed that the impurity levels are higher within the carbon fibres than in the CVD carbon coating. As examples, Fig. 12a and b shows SIMS digital mapping for Ca and Ti, respectively, on CVD CBCF samples. In some cases evidence was also provided for a tendency for impurities to become concentrated at the fibre surface/interfacial region or, to usually a lesser extent, the pyrocarbon coating surface. This is well illustrated in Fig. 12b, where a higher concentration of titanium can be seen at the fibre and coating surfaces (as indicated by arrows).

3.3. Requirements for successful SiC deposition

As indicated earlier, silicon carbide deposition is more successful with CVD CBCF than with CBCF. A number of possible explanations for this behaviour have come to light during this investigation, namely the comparative purity, roughness, and crystallinity of the two substrate materials.

The CVD CBCF substrate was found to have a higher level of purity than the CBCF material (a consequence of the high purity pyrocarbon coating) using neutron activation analysis (see Table 2) and secondary ion mass spectrometry (see Table 3). SIMS depth profiling and digital mapping have demonstrated that the impurities may be concentrated at the fibre surface, and also sometimes, but to a lesser extent, at the pyrocarbon surface (see Figs. 11 and 12). Impurities on the fibre surface will interfere with the chemical reactions taking place during any attempted silicon carbide deposition. The interference will depend on the level and type of impurity and whether the impurity is able to diffuse through the SiC coating to the top of the coating where it will be active or whether it will become encapsulated by the SiC coating. It is generally accepted that in most instances impurities in the substrate are not an advantage in CVD as they may lead to different local reaction rates,[8] yield compounds which alter the layer structure locally[9] and, in extreme cases, could even change materials from the solid form into the liquid form (liquid phase epitaxy is well known).[10] These side effects are extremely unpredictable and depend on many global and local factors in the reactor system. Thus, the impure surface of the CBCF could be hindering the deposition of silicon carbide, whereas the

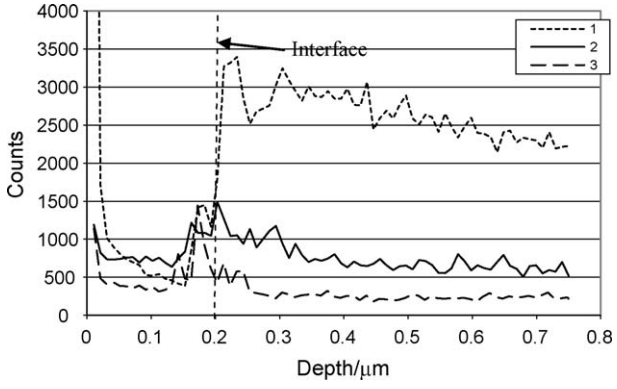

Fig. 11. SIMS depth profiling for calcium conducted on fibres within CVD CBCF, showing three typical traces.

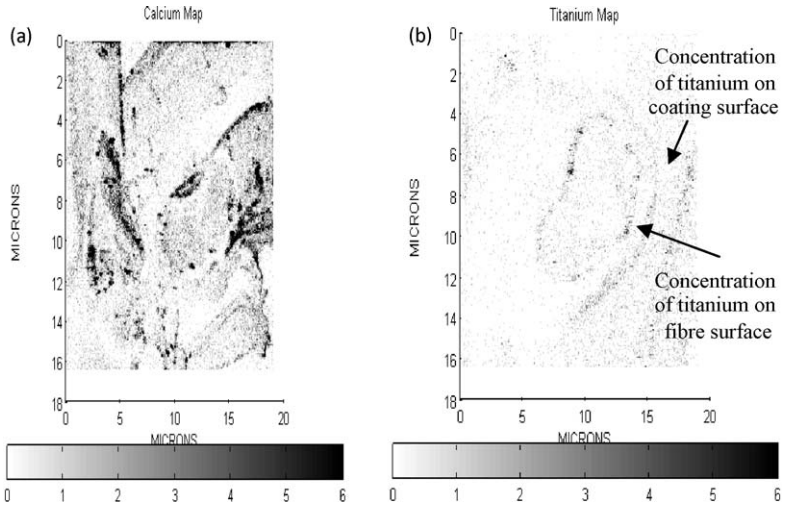

Fig. 12. SIMS digital mappings for the CVD CBCF sample, showing (a) levels of calcium and (b) levels of titanium.

effectiveness of the CVD carbon coating in promoting a good quality SiC coating may, in part, be due to its high purity.

The pyrocarbon layer was seen to be more crystalline/structured than the carbon fibre itself using high resolution TEM images (Fig. 7) as well as electron diffraction (Fig. 8). The fact that the pyrocarbon coating is more crystalline than the carbon fibres could also affect the deposition process and nature of the deposit. For CVD silicon carbide deposited on silicon carbide wafers using a MTS precursor gas, Lu et al.[11] reported that the deposits differed according to the level of misorientation within the silicon carbide wafer substrates. The substrates used were 6H- and 4H-SiC (0 0 0 1) wafers with different misorientation (<0.5°, 3.5° and 8°) tilts towards $(1\,1\,\bar{2}\,\bar{0})$. With the silicon carbide wafer substrates with <0.5° misorientation, 3C-SiC was deposited, whereas when the misorientation in the wafers was highest (8°), the deposits perfectly replicated the substrate polytypes (i.e. either 4H- or 6H-SiC). For substrate misorientation of 3.5°, mixtures of 3C- and 6H-SiC were produced. In terms of the effect of substrate crystallinity on other CVD deposited materials, Ward et al.[12] reported that the substrate crystallinity influenced the growth and nucleation of single walled nanotubes (SWNT) grown using CVD, the yield of SWNT was greater the more crystalline the substrates. In Ref. [13], the influence of germanium substrate crystallinity on the formation of cobalt germanide thin films was investigated. It was found that the deposition temperatures required were lower with amorphous substrates. It may be concluded from these studies that the degree of crystallinity and the orientation of a substrate affects CVD deposition and it is likely that the greater crystallinity of the pyrocarbon is beneficial for the deposition of SiC.

The surface of the CVD CBCF (coated fibre) is rougher than that of the CBCF (uncoated fibre), as shown in Table 1. A rough surface should improve coating adhesion, and in the case of CVD a rougher substrate could promote also a more uniform coating. The density of initial crystals adhered to the substrate surface affect the uniformity of coatings, as with fewer crystals adhering, it is likely that a non-uniform or patchy coating would be yielded. In terms of the deposition of a coating, this is also linked to the bulk density of the coating, as a patchy deposition will result in a porous coating. Indeed adhesion, uniformity and density are all features of the coating quality. Evidence for the effect of substrate roughness on coating density can be found, for example, in Ref. [14] where silicon carbide films were deposited on both rough and smooth mullite substrates. It was reported that dense films were deposited on the rougher surfaces and porous films on the smooth surfaces. Based on this result, it can be said that the fact that the CVD CBCF surfaces are rougher will probably make this material more amenable to the deposition of good quality silicon carbide than the base CBCF material.

The three factors investigated have shown the CVD CBCF material as being considerably more suitable to silicon carbide deposition than the uncoated CBCF substrate. It could be one factor by itself which leads to successful deposition of silicon carbide within CVD CBCF or a combination of two or more of the various factors investigated. Another factor which may play a major role is the residual thermal stresses generated as a result of the CVD process, but detailed consideration of residual thermal stresses generated as a result of the CVD of silicon carbide onto both CBCF and CVD CBCF substrates is beyond the scope of the present study. It is anticipated that a theoretical model predicts that the generated stresses are significantly lower with the CVD CBCF substrate, as the pyrocarbon layer has an intermediate thermal expansion coefficient when compared to the carbon fibres and silicon carbide coating, which would thus favour the production of a sound SiC deposit.

4. Conclusions

SiC coated CBCF materials were investigated. The as-received silicon carbide coating is uniform with few flaws and thus is likely to be effective in preventing degradation of the base CBCF material. The average thickness of the silicon carbide coating is approximately 1 μm. It consists of two regions of β silicon carbide: a fine polycrystalline region (~0.3 to 0.4 μm) out of which large columnar grains (~0.5 μm) grow.

The pyrocarbon in CVD CBCF is more crystalline and purer than the underlying carbon fibres. Furthermore, CVD CBCF has a rougher surface than the uncoated CBCF. The XMT study has provided information about fibre orientations (random within *x*/*y* layers, but a tendency for less fibres orientated at angles 40–100° in the planes perpendicular to these layers (*z* plane)) which is in good agreement with a previous study on the fibre orientations of CBCF materials, conducted using optical microscopy. Based on this study a number of explanations have been put forward for the successful deposition of silicon carbide when CVD CBCF is used as the substrate material as opposed to the base CBCF material. These are:

(i) the increased crystallinity of the pyrocarbon coating,
(ii) the greater roughness of the CVD CBCF substrate surface,
(iii) the higher purity of the CVD CBCF surface,
(iv) the lower residual thermal stresses in the presence of the pyrocarbon layer (this will be demonstrated in a subsequent publication).

Acknowledgements

The authors express their thanks to the EPSRC for funding the project and Calcarb Ltd. for additional funding as well as the supply of materials. In addition, Richard Chater and Mahmoud Ardakani at the Department of Materials, Imperial College, are acknowledged for help with SIMS/Zygo and TEM, respectively and Professor Peter D. Lee (Imperial College) for allowing the use of the XMT facility.

References

1. Davies IJ, Rawlings RD. Microstructural investigation of low-density carbon–carbon composites. *Journal of Materials Science* 1994;**29**(2): 338–44.
2. Davies IJ, Rawlings RD. Mechanical properties in flexure of CVI-densified porous carbon–carbon composites. In: *Proceedings of the ECCM-7 conference*. 1996. p. 449–54.
3. Davies IJ, Rawlings RD. Mechanical properties in compression of CVI-densified porous carbon/carbon composite. *Composites Science and Technology* 1999;**59**(1):97–104.
4. Westwood ME, Webster JD, Day RJ, Hayes FH, Taylor R. Oxidation protection for carbon fibre composites. *Journal of Materials Science* 1996;**31**(6):1389–97.
5. Sibieude F, Benezech G. Chemical vapour deposition of silicon carbide: an X-ray diffraction study. *Journal of Materials Science* 1988;**23**(5):1632–6.
6. Lespiaux D, Langlais F, Naslain R, Schamm S, Sevely J. Correlations between gas phase supersaturation, nucleation process and physico-chemical characteristics of silicon carbide deposited from Si–C–H–Cl system on silica substrates. *Journal of Materials Science* 1995;**30**(6):1500–10.
7. Davies IJ, Rawlings RD. Effect of recycled material on the structure and properties of low density carbon–carbon composites. In: *Proceedings of the ECCM-6 conference*. 1993. p. 553–8.
8. Nishi Y, Doering R. *Handbook of semiconductor manufacturing technology*. New York: Marcel Dekker; 2000.
9. Microelectronic materials and processes.Levy RA, editor. *Proceedings of the NATO advanced study institute on microelectronic materials and processes*. Castelvecchio Pascoli, Italy: Springer; 1989.
10. Dmitriev V, Cherenkov A. Growth of SiC and SiC–AlN solid solution by container-free liquid phase epitaxy. *Journal of Crystal Growth* 1993;**128**(1–4):343–8.
11. Lu P, Edgar JH, Glembocki OJ, Klein PB, Glaser ER, Perrin J, Chaudhuri J. High-speed homoepitaxy of SiC from methyltrichlorosilane by chemical vapor deposition. *Journal of Crystal Growth* 2005;**285**(4):506–13.
12. Ward JW, Wei BQ, Ajayan PM. Substrate effects on the growth of carbon nanotubes by thermal decomposition of methane. *Chemical Physics Letters* 2003;**376**(5–6):717–25.
13. Opsomer K, Deduytsche D, Detavernier C, Van Meirhaeghe RL, Lauwers A, Maex K, Lavoie C. Influence of Ge substrate crystallinity on Co germanide formation in solid-state reactions. *Applied Physics Letters* 2007;**90**:031906.
14. Regiani I, de Souza MF. Silicon carbide coating of mullite substrates by the CVD technique. *Surface and Coatings Technology* 2003;**162**(2–3):131–4.